Alkalinization by chloride/bicarbonate pathway in larval mosquito midgut

Dmitri Y. Boudko*, Leonid L. Moroz, William R. Harvey, and Paul J. Linser

The Whitney Laboratory, University of Florida, St. Augustine, FL 32086

Edited by John H. Law, University of Arizona, Tucson, AZ, and approved September 26, 2001 (received for review May 21, 2001)

The midgut of mosquito larvae maintains a specific lumen alkalinization profile with large longitudinal gradients (pH ≈ 3 units·mm^{-1}) in which an extremely alkaline (pH ≈ 11) anterior midgut lies between near-neutral posterior midgut and gastric cecum (pH 7–8). A plasma membrane H^+ V-ATPase energizes this alkalinization but the ion carriers involved are unknown. Capillary zone electrophoresis of body samples with outlet conductivity detection showed a specific transepithelial distribution of chloride and bicarbonate/carbonate ions, with high concentrations of both anions in the midgut tissue: 68.3 ± 5.64 and 50.8 ± 4.21 mM, respectively. Chloride was higher in the hemolymph, 57.6 ± 7.84, than in the lumen, 3.51 ± 2.58, whereas bicarbonate was higher in the lumen, 58.1 ± 7.34, than the hemolymph, 3.96 ± 2.89. Time-lapse video assays of pH profiles *in vivo* revealed that ingestion of the carbonic anhydrase inhibitor acetazolamide and the ion exchange inhibitor DIDS (4,4′-diisothiocyanatostilbene-2,2′-disulfonic acid), at 10^{-4} M eliminates lumen alkalinization. Basal application of these inhibitors *in situ* also reduced gradients recorded with self-referencing pH-sensitive microelectrodes near the basal membrane by ≈65% and 85% respectively. Self-referencing chloride-selective microelectrodes revealed a specific spatial profile of transepithelial chloride transport with an efflux maximum in anterior midgut. Both acetazolamide and DIDS reduced chloride effluxes. These data suggest that an H^+ V-ATPase-energized anion exchange occurs across the apical membrane of the epithelial cells and implicate an electrophoretic Cl^-/HCO_3^- exchanger and carbonic anhydrase as crucial components of the steady-state alkalinization in anterior midgut of mosquito larvae.

The human stomach works at an acid pH near 1, whereas the larval mosquito midgut works at an alkaline pH near 11. The acid pH of mammalian stomachs has been thoroughly investigated and its mechanisms are understood in great detail. The alkaline pH of larval mosquito midguts has been little studied and remains largely a mystery. Recently developed techniques for direct analysis of the intact midgut *in vivo* and in semi-intact larvae, with a resolution that allows analytical assay of small patches of tissue, even of individual cells, have led to insights into the alkalinization mechanism.

The principal function of the larval mosquito midgut is to digest and absorb nutrients. High pH values have been recorded in anterior midgut of several mosquito larvae, including *Aedes aegypti* (1), as well as in some lepidopteran larvae with high tannin diet (2). The alkaline environment of the anterior midgut lumen enhances dissociation of tannin–protein complexes and, therefore, would be advantageous for the nutrition of herbivorous and detritus-feeding larvae (3). The tannin-free protein could then be digested and absorbed at the near neutral pH of posterior midgut lumen (3, 4). This pattern of nutrient processing has led to the large longitudinal gradients of pH and ionic concentration. How can such a large pH gradient be generated over short distances in the absence of morphological barriers? Apparently, it is the result of region-specific ion transport. It is established that this transport is energized by a plasma membrane H^+ V-ATPase (5–7), but the ion transporters involved are heretofore unknown.

An H^+ V-ATPase is expressed in anterior midgut of mosquito larvae (5), where it was immunolocalized with a subunit E specific antibody at the basal plasma membranes of epithelial cells (7). Region-specific pH gradients emanating from the midgut of fourth instar *A. aegypti* were detected by using self-referencing ion-selective liquid ion exchanger (SERIS-LIX) microelectrodes, with the largest acid secretion in anterior midgut (6). The specific H^+ V-ATPase inhibitor bafilomycin A dramatically reduced the pH gradients and lumen alkalinization, indicating that both processes are coupled to H^+ V-ATPase activity (6). To achieve a pH of 11, strong cations, such as Na^+ or K^+, and weak anions, such as OH^-, CO_3^{2-}, or HCO_3^-, must be accumulated in the lumen of anterior midgut. Thus, two epithelial transport pathways are implied for the alkalinization: a cationic pathway, in which a strong cation replaces a weak one, and/or an anionic pathway, in which a weak anion replaces a strong one in the midgut lumen. Our preliminary studies with Na^+- and K^+-selective SERIS–LIX probes indicated only minor fluxes of those cations in anterior midgut. We used pharmacological modulators of cation transport *in situ* and *in vivo* and found no evidence that cationic pathways are crucial for the steady-state alkalinization (data not shown). In contrast, strong chloride fluxes and specific patterns of transepithelial chloride/bicarbonate distribution were found. Here we present evidence that an anionic pathway is important for the alkalinization of anterior midgut of *A. aegypti* larvae.

Materials and Methods

Experimental Procedures. Early and middle fourth instar larvae of *A. aegypti* were reared from eggs (courtesy of the United States Department of Agriculture, Gainesville, FL) in 2% artificial seawater (ASW, consisting of 8.4 mM NaCl, 1.7 mM KCl, 0.1 mM $CaCl_2$, 0.46 mM $MgCl_2$, 0.51 mM $MgSO_4$, and 0.04 mM $NaHCO_3$). To obtain physiologically homogenous populations, larvae were grown in a low-temperature incubator (Fisher Scientific) at 20°C with a 12-h light period. Measurements of ionic gradients were performed in hemolymph-substitute medium (HSM, consisting of 42.5 mM NaCl, 3.0 mM KCl, 0.6 mM $MgSO_4$, 5.0 mM $CaCl_2$, 5.0 mM $NaHCO_3$, 5.0 mM succinic acid, 5.0 mM malic acid, 5.0 mM L-proline, 9.1 mM L-glutamine, 8.7 mM L-histidine, 3.3 mM L-arginine, 10.0 mM dextrose, 25 mM Hepes, pH adjusted to 7.0 with NaOH). All chemicals were obtained from Sigma. Inhibitors were used as HSM or 2% ASW solutions prepared from stock, 0.2–1 M of a ligand in DMSO. *m*-Cresol purple (1%) was prepared in DMSO and diluted as required.

This paper was submitted directly (Track II) to the PNAS office.

Abbreviations: ASW, artificial seawater; CZE, capillary zone electrophoresis; SERIS, self-referencing ion-selective; LIX, liquid ion exchanger; CA, carbonic anhydrase; HSM, hemolymph-substitute medium; DIDS, 4,4′-diisothiocyanatostilbene-2,2′-disulfonic acid.

*To whom reprint requests should be addressed. E-mail: boudko@whitney.ufl.edu.

The publication costs of this article were defrayed in part by page charge payment. This article must therefore be hereby marked "*advertisement*" in accordance with 18 U.S.C. §1734 solely to indicate this fact.

www.pnas.org/cgi/doi/10.1073/pnas.261253998

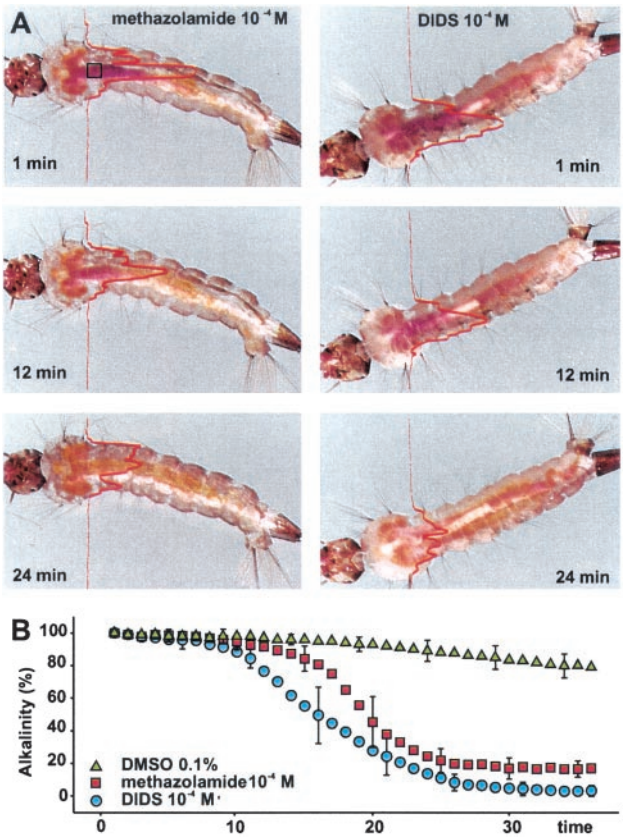

Fig. 1. Time-lapse monitoring of alkalinity profile in intact larvae. (*A*) Images extracted from time-lapse video recordings of fourth-instar *A. aegypti*. Dye intensity in the presence of 10^{-4} M methazolamide (*Right*) or in the presence of 10^{-4} M DIDS (*Left*). The lines through the images represent the relative optical density profile on a magenta channel (NIH IMAGE). The dark purple staining in anterior midgut in the 1-min frame corresponds to a pH value above 10. By 24 min, the pH has declined and approaches 7. The pH values in the referenced points were confirmed with pH-sensitive glass microelectrodes (11.1 ± 0.2). (*B*) Time course of midgut dealkalinization after addition of methazolamide and DIDS. Error bars represent SD value of every fifth time-lapse sample ($n \geq 4$).

Time-Lapse Assay of Midgut Alkalinization *in Vivo*. Midgut alkalinization profiles were visualized in intact larvae that had ingested an indicator solution (0.04% *m*-cresol purple in 2% ASW) with or without an inhibitor. Labeled larvae were mechanically immobilized in a small volume of 2% ASW between a microscope slide and a patch of acetate film. Time-lapse video clips were acquired on a Pentium computer using an Olympus SZX-12 stereomicroscope equipped with a Pixera Professional charge-coupled device camera (World Precision Instruments, Sarasota, FL). Selected frames were extracted from the AVI file and separated to CMYK channels by using Corel PHOTO-PAINT software (Corel, Ottawa, Canada). A magenta channel (8-bit gray level), that matched the pH-dependent color transient of *m*-cresol purple, was stored as a TIF bitmap and analyzed. A linear OD profile through the larva, which represents an alkalinization profile of the midgut, was scanned from the TIF frames (Fig. 1*A*) by using a line profile tool of Scion IMAGE software (PC version of NIH IMAGE, Scion, Fredrick, MD). Positions versus arbitrary OD values were analyzed by using SIGMA PLOT software (SPSS, Richmond, CA). Maximum OD values from individual frames were normalized relative to the minimal intensity of purple color in anterior midgut.

Collection of Tissue and Body Fluid Samples. Cold-immobilized larvae were attached to a Sylgard-coated dish, blotted with filter paper, and covered with mineral oil. The larval cuticle was slit. Hemolymph was collected with a glass capillary between two concave hemispherical plugs of mineral oil. The sample volume was calculated as an equivalent cylinder with radius, *r*, and length, *l*, from which two hemispheres are removed:

$$V = \pi r^2 l - \frac{4}{3}\pi r^3. \quad [1]$$

A sample of peritrophic fluid was collected from the intact gut by using a similar technique except that a fused silica capillary (100 μm i.d.), which was prefilled with mineral oil and connected to a GENIE-programmed syringe pump (World Precision Instruments), was used. The samples were extruded onto a piece of Parafilm tape and diluted with HPLC-grade deionized water. A sample of midgut contents was collected from the anterior part of the larval midgut and dialyzed in a 1,000-fold excess volume of capillary electrophoresis-grade deionized water. Anterior midgut tissue was dissected in HSM, separated from lumen contents, blotted with filter paper, immersed in deionized water, and homogenized by freezing and ultrasonic agitation. All samples were centrifuged before injection to reduce the possibility of capillary contamination.

Capillary Zone Electrophoresis (CZE). The computer-controlled setup included a PrinCE system (Prince Technologies, Emmen, The Netherlands) and Crystal-1000 suppressed conductivity detector (Thermo Bioanalysis, Waltham, MA). A fused silica capillary, 50 μm i.d. and 70 cm long, was used. CZE data were collected with a 20-bit acquisition board. PrinCE controls, calibration, data collection and analyses were performed by using DAX software (Van Mierlo Software Consultancy, Eindhoven, The Netherlands).

The experimental protocol was optimized for analysis of submicromolar concentrations of inorganic anions in nanoliter samples. The background electrolyte, arginine/borate buffer consisted of 25 mM arginine, 81.5 mM borate, and 0.5 mM tetradecyltrimethylammonium hydroxide, an electro-osmotic flow modifying solution. The buffer pH was adjusted to 9.5 with NaOH.

Precautions were taken to avoid artifacts in the determination of carbonic acid products: (*i*) no stacking leader solution was used, (*ii*) the sample was analyzed immediately after isolation, and (*iii*) a correction for background bicarbonate/carbonate was made by subtracting the value detected in a deionized water sample from those found in biological samples and calibration solutions of anions. Samples were loaded by pressure, 60-mbar (1 mbar = 100 Pa) for 6 s. The separation voltage was −20 kV. The CZE system and capillary were thermostabilized at 16°C. Anions were identified by their apparent mobility. A three-point calibration was used to determine the concentration for each species. The injection volume was calculated according to the equation for hydrodynamic injection (8).

Midgut Preparation. Noninvasive assays of pH and chloride gradients were made on intact midgut preparations within semi-intact larvae, as described (6). In these preparations the midgut retains natural epithelial functions, including normal midgut alkalinization, for many hours. Recordings were carried out at room temperature (23 ± 1°C). Preparations were allowed to stabilize for ≈5 min after dissection and before recording.

Noninvasive Assay of Ion Fluxes with Self-Referencing Ion-Selective (SERIS) Microelectrodes. Gradients of pH and chloride activity were measured by using SERIS-LIX microelectrodes as described (6, 9). The pH ionophore-I mixture B and Cl^- ionophore-I mixture A were purchased from Fluka. The optimal parameters for preparation of LIX and reference electrodes

PHYSIOLOGY

were established empirically (9). Slope values were 58 ± 1.2 and −59.3 ± 1.5, and selectivity coefficients relative to possible interfering ions were <-9 and <-5.2 for pH-LIX and Cl^--LIX probes respectively. The collected data were exported into an EXCEL 2000 spreadsheet format (Microsoft), then analyzed and visualized with SIGMA PLOT 5.

Ion Activity Gradient, Δ*a*(I), and Flux (*J*) Calculations. Probe-motion related differences of ion activity $\Delta a(\mathrm{I})$ were calculated from the SERIS-LIX probe signal ΔV, by using the probe slope value S from calibrations and average ion activities recorded in the bathing solution during experiments, $a(\mathrm{I})_{av}$ (9):

$$\Delta a(\mathrm{I}) = a(\mathrm{I}_{av})10^{\Delta V/S} - a(\mathrm{I}_{av}). \quad [2]$$

Ion fluxes (J) were calculated from Fick's first law, the equation for nonelectrolytes. Rather than attempting to integrate the Nernst–Planck equation for the complex ion flux (J), the effects of the electrical field on ionic diffusion were taken into account by means of an experimentally determined correction coefficient, C_f (9):

$$J = -\frac{C_f D\, a(\mathrm{I}_{av})}{\Delta l}(10^{\Delta V/S} - 1), \quad [3]$$

where D is a diffusion coefficient ($m^2 \cdot s^{-1}$) and Δl is the probe excursion distance (m). To calculate basal acid/base fluxes (H^+ mol equivalent$\cdot m^{-2} \cdot s^{-1}$) at the interface with a buffered medium such as HSM, thermodynamic and buffer-facilitated proton movements were taken into account (10). To avoid the necessity of estimating the buffer diffusion constant (10) our calculation was based on a recently published equation (11) modified to consider the correction for the electrical field effect, C_f (9), and for the presence of multiple pH buffering compounds in the solution:

$$J_H = -\frac{D_H \Delta a(H^+)}{\Delta l}\left(C_f + \sum_{i=1}^{n}\frac{0.25[B_i]}{K_{a_i}}\right), \quad [4]$$

where J_H, is the acid/base flux (mol$\cdot m^{-2} \cdot s^{-1}$); D_H, is the hydrogen ion diffusion constant; $\Delta a(H^+)$, is the basal hydrogen ion activity gradient (Eq. **2**); n is the buffering compounds number; [B] is the buffer concentration expressed in mol$\cdot m^{-3}$, and K_a is the dissociation constant. The constants used were: $D_{Cl-} = 2.03 \times 10^{-9}$ $m^2 \cdot s^{-1}$; $D_{H+} = 9.31 \times 10^{-9}$ $m^2 \cdot s^{-1}$; Hepes $pK_a = 7.56$; diprotic carbonic acid $pK_{a1} = 6.35$; and bicarbonate $pK_{a2} = 10.33$ (8).

Results

Midgut Alkalinization *in Vivo*. The anterior midgut exhibits the highest luminal pH as indicated by intense purple labeling with *m*-cresol purple. Time-lapse monitoring of the pH profile with this indicator confirmed a gradual decay of alkalinization in the anterior midgut of mechanically immobilized larvae, with 4–6 h being required for complete neutralization ($n = 12$)., Larvae that were freed from immobilization rapidly re-established midgut alkalinization, normal swimming/feeding behavior, and ability to pupate ($n = 12$). Immobilized larvae retain only minor swimming movements. By contrast, activity in the labial complex and the ratio of peristaltic movements in midgut to that in tracheal trunks were similar to the values observed in free-swimming larvae. When larvae were placed in 2% ASW containing 10^{-4} M methazolamide, a carbonic anhydrase (CA) inhibitor, or 10^{-4} M DIDS, which inhibits ionic exchanges, including Cl^-/HCO_3^- exchange, the alkalinity declined rapidly ($n = 4$ and 5, respectively, Fig. 1). No significant differences of the alkalinization time courses were observed between larvae in pure 2% ASW and that substituted with 0.1% DMSO ($n = 4$; paired t test, $P < 0.0001$).

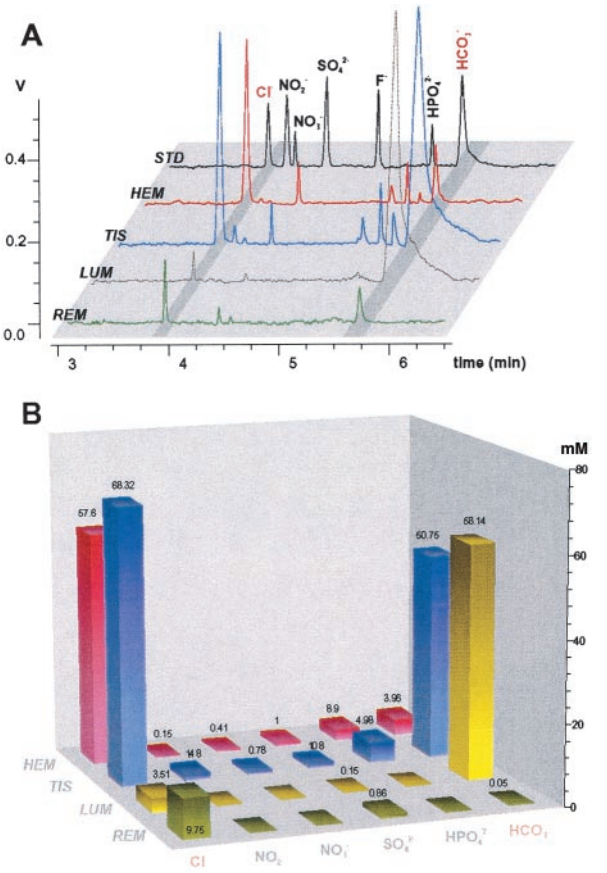

Fig. 2. CZE analyses of anions in mosquito body samples with outlet conductivity detector. (*A*) Orthogonal overlay of typical electropherograms from subset of biological samples. *REM*, rearing media; *LUM*, ectoperitrophic fluid (lumen) sample from the anterior midgut area; *TIS*, anterior midgut tissue sample; *HEM*, hemolymph; *STD*, 2-ppm mixture of anion standards. *z* axis signal from conductivity detector, V (scale setting of 1 V corresponds to 100 μS). (*B*) The absolute values of ion concentrations were estimated by using peak areas and slope values from standard solutions. The *z* axis is the estimated ion concentrations in undiluted samples in mM. Numbers above bars are mean values of the determined concentrations ($n \geq 3$, for all values shown).

Concentrations of Anions in Anterior Midgut. The optimal conditions for detection and separation of inorganic anions were achieved in a buffer consisting of 25.0 mM arginine, 81.5 mM borate, and 0.5 mM TTAOH, pH 9.5. A 1,000-fold sample dilution and 6.6-nl injection volume of the diluted sample were found optimal for reliable determinations of inorganic anions in the samples (Fig. 2*A*). Anions were identified by their electrophoretic migration time, in min, as follows: Cl^-, 3.8946 ± 0.0015; NO_2^-, 4.0604 ± 0.0020; NO_3^- 4.1328 ± 0.0024; SO_4^{2-}, 4.4248 ± 0.0029; F^-, 4.8979 ± 0.019 (internal standard); HPO_4^{2-}, 5.3787 ± 0.0024; HCO_3^-, 5.6498 ± 0.0035 (all $n \geq 4$). The "HCO_3^-" peak obviously represents a mixture of HCO_3^- and CO_3^{2-} and is termed the carbonate/bicarbonate peak.

Samples obtained from anterior midgut endoperitrophic contents and ectoperitrophic fluid had similar concentrations of inorganic anions ($n = 3$ and 6, respectively) and are referred to hereafter as luminal samples. The highest chloride concentration was found in the anterior midgut tissue, 68.3 ± 5.9 mM (mean ± SD, $n = 5$) (Fig. 2*B*). The hemolymph chloride concentration

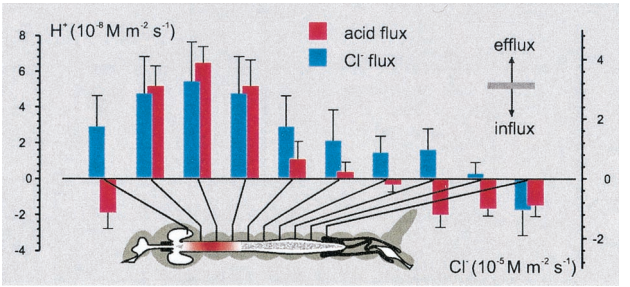

Fig. 3. Regional specificity of transepithelial chloride and acid fluxes in midgut of fourth-instar *A. aegypti*. (*Inset*) SERIS-LIX probe positions for each bar of the histogram. Bars are flux values calculated from Eqs. **3** and **4** ($J \pm$ SD).

was significantly different from that in the tissue, 57.6 ± 5.7 mM ($n = 5$, paired t test, $P = 0.00013$). By contrast, an extremely low chloride concentration was detected in luminal fluid, 3.51 ± 2.58 mM ($n = 4$). The transepithelial bicarbonate/carbonate distribution profile was the inverse of that of chloride. The carbonate/bicarbonate concentration was highest in the anterior midgut lumen, 58.1 ± 4.81 mM ($n = 5$). Tissue concentration of these ions was lower than and significantly different from those in the lumen, 50.7 ± 4.15 mM ($n = 5$; paired t test, $P = 0.00035$). Surprisingly low bicarbonate concentrations were found in hemolymph samples, 3.96 ± 2.89 mM ($n = 4$). Other major inorganic anions that were reliably determined in the biological samples from mosquito larvae were NO_2^-, NO_3^-, SO_4^{2-}, and HPO_4^{2-} (Fig. 2*B*).

Profiles of Acid and Chloride Fluxes. The pH gradient (ΔpH) profiles around the midgut of *A. aegypti* larvae were similar to those described earlier (6). Here we present the spatial profile of transepithelial acid/base transport as fluxes of an H^+ equivalent (Fig. 3). Corrections for media with pH buffer were performed according to a recently published equation (11). The largest acid efflux was in the anterior midgut area, 64.6 ± 9.24 nM·m^{-2}·s^{-1} ($n = 14$, Fig. 3), and corresponds to the area of the highest luminal pH. The largest Cl^- efflux, 32.6 ± 1.32 μM·m^{-2}·s^{-1} ($n = 8$, Fig. 3), was also found in anterior midgut and corresponds to the area of the largest transepithelial acid efflux (Fig. 3). In contrast to the H^+ and Cl^- efflux recorded in anterior midgut, H^+ and Cl^- influx was recorded near a Malpighian tubule loop ($n = 5$). In gastric ceca and posterior midgut, the H^+ and Cl^- fluxes were in opposite directions (Fig. 3).

Pharmacological Properties of Acid Efflux. The effects of DIDS, acetazolamide, and DMSO were monitored in the middle of the anterior midgut, at the point of the largest acid efflux, which was established by lateral screening of each individual preparation with the SERIS-LIX probe before pharmacological treatment. The flux values were steady for about 4 h (maximum recording time attempted on control preparations) and were not significantly affected by the basal administration of 0.1% DMSO (Fig. 4). Basal application of the membrane-permeant CA inhibitors acetazolamide and methazolamide reduced the acid efflux in a concentration-dependent manner (Fig. 4 *A* and *C*). The maximum effect, about 65% inhibition (normalized to preceding values), was attained at concentrations ≥10^{-4} M. Similar effects were recorded after addition of methazolamide, except that the inhibition was faster and the concentration threshold for maximum inhibition was lower, ≈10^{-5} M (Fig. 4*C*). By contrast, the weaker membrane-permeant benzolamide at 100-μM concentrations had no significant effects on the anterior midgut pH gradients (data not shown). Basal application of DIDS reduced the acid efflux in a concentration-dependent manner (Fig. 4 *B*

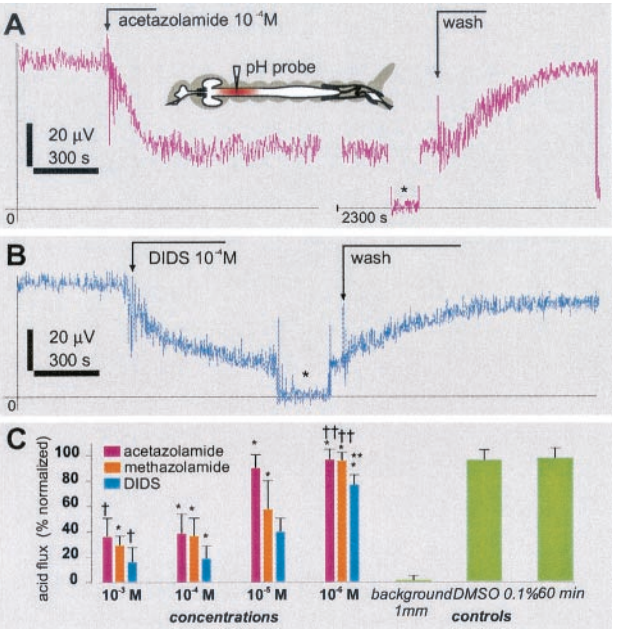

Fig. 4. Pharmacological effects of acetazolamide, methazolamide, and DIDS on acid efflux in the anterior midgut of mosquito larvae. (*A* and *B*) Time course of SERIS-pH-LIX probe readings during basal application of acetazolamide (*A*) and DIDS (*B*). Broken arrows indicate events during recording. *, A background signal at 1 mm from the tissue. (*Inset*) The approximate position of the recording probe. (*C*) Normalized dose–response histogram of acid efflux inhibition. Bars are mean ± SD ($n \geq 4$ for each concentration). *, A significant difference of the value compared with a value from the preceding 1:10 dilution (paired t test, $P > 0.001$ for all significant definitions); †, insignificant differences of the value compared with the value from the preceding 1:10 dilution; **, significant differences compared with 0.1% DMSO and 30-min controls; ††, insignificant difference compared with the controls.

and *C*). Maximum inhibition of ≈85% was obtained with DIDS concentrations ≥10^{-4} M. The effects of acetazolamide, methazolamide, and DIDS were partly reversible (Fig. 4) and repeatable.

Pharmacological Properties of Cl^- Efflux. Basal application of amides and DIDS induced a concentration-dependent decay of Cl^- efflux in the anterior midgut (Fig. 5). Surprisingly, at 10^{-4} M, DIDS induced a small reversal of chloride flux ($n = 4$). The DIDS effects were partly reversible on washout but complete recovery was never observed. The minimal concentration that induced a significant decay of chloride efflux was 10^{-6} M (t test, $P > 0.001$). Methazolamide significantly inhibited the chloride efflux at ≥10^{-5} M (t test, $P > 0.0001$) but did not produce significant changes at 10^{-6} M. In contrast to DIDS, a reversal of the chloride flux was never observed with methazolamide. The effects of methazolamide on the chloride efflux were reversible, and in some cases the value after washout exceeded the average value preceding drug administration (3 of $n = 12$, Fig. 5 *A* and *C*). Reversible inhibition by methazolamide and DIDS could be repeated several times on the same midgut preparation.

Discussion

Our evidence for an anion exchanger in anterior midgut of fourth-instar mosquitoes provides fresh insight into an old mystery. Since the early 1900s, when high luminal alkalinity in larval mosquito midgut (12) and caterpillar midgut (13) were initially reported, the mechanism by which this high pH (14) is attained has intrigued biologists. In the caterpillar *Manduca sexta*, midgut alkalinization is thought to be achieved by means of the combined action of an electrogenic H^+ V-ATPase and an

PHYSIOLOGY

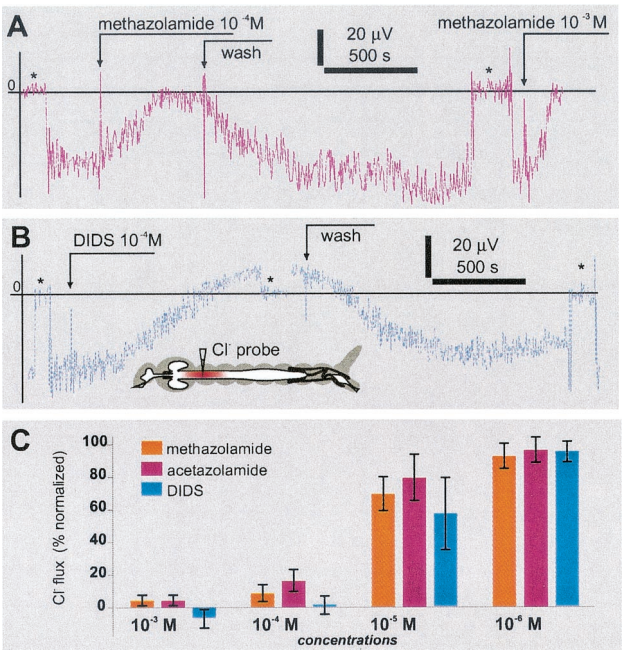

Fig. 5. Pharmacological effects of methazolamide and DIDS on chloride effluxes in the anterior midgut of mosquito larvae. (*A* and *B*) Time course of SERIS-Cl^--LIX probe readings during basal application of methazolamide (*A*) and DIDS (*B*). Broken arrows indicate events during recording. Asterisks indicate a background signal at 1 mm from the tissue. (*C*) Normalized dose–response histogram of Cl^- efflux inhibition. Bars are mean ± SD ($n \geq 4$ for each concentration).

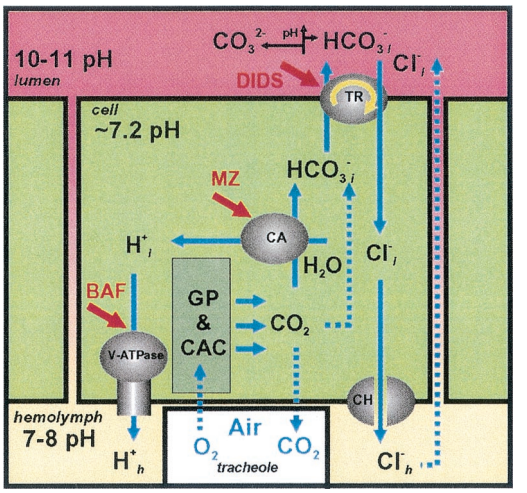

Fig. 6. Diagram of hypothetical midgut alkalinization (see *Discussion*). The deduced locations of the membrane-energizing H^+ V-ATPase, the proton- and bicarbonate-supplying CA, and the putative voltage-driven Cl^-/HCO_3^- anion exchanger are shown. The most effective inhibitors of the pathway are bafilomycin A (BAF), methazolamide (MZ), and DIDS. GP, glycolytic pathway; CAC, citric acid cycle.

electrophoretic $K^+/2H^+$ antiporter (15). The plasma membrane H^+ V-ATPase is well established (review in ref. 16), but the cation antiporter and other components of the ionic pathway remain enigmatic, despite extensive efforts toward their identification (17). Recently, the H^+ V-ATPase-coupled, cationic mechanism was challenged on the thermodynamic grounds that it is insufficient to produce the recorded high midgut alkalinity (18–20).

The presence of a V-ATPase is also well established in anterior midgut of mosquito larvae (5), where its localization in the basal plasma membrane (7) is consistent with electrical measurements of large transbasal potentials (21, 22) and where it apparently energizes anterior midgut alkalinization (6). Despite extensive efforts, no cationic fluxes related with alkalinization were identified (data not shown). In contrast, significant chloride effluxes accompanied by acid secretion in anterior midgut were found. We report here evidence from (*i*) pharmacological analysis of midgut alkalinization *in vivo* with time-lapse assay of pH profiles, (*ii*) evaluation of transepithelial ion distributions by CZE of larval body samples, and (*iii*) measurement of Cl^- and pH gradients with ion-selective SERIS-LIX microelectrodes *in situ*, which show that an anionic pathway plays a major role in the alkalinization of anterior midgut lumen and implicate CA and a Cl^-/HCO_3^- exchanger as two important components of the pathway. CA has recently been cloned from midgut cDNA samples of fourth-instar *A. aegypti* and detected in midgut tissue by histochemical techniques and *in situ* hybridization and by biochemical assays of enzyme activity (M. del Pilar Corena and P.J.L., unpublished results). A Na^+-driven Cl^-/HCO_3^- exchanger has been cloned, characterized, and detected by *in situ* hybridization in the alimentary system of another dipteran larva, *Drosophila melanogaster* (23).

Time-lapse analyses of living larva revealed that CA and anion exchanger activity are crucial for anterior midgut alkalinization (Fig. 1). This method combined sophisticated time-lapse video recording and optical density scanning with the pH dye technique of Dadd (1, 24).

Strong acid and chloride effluxes were recorded with noninvasive pH- and Cl^--sensitive SERIS-LIX probes from the basal surface of anterior midgut (Fig. 3). These observations are consistent with the highest luminal pH being found in anterior midgut, provide direct confirmation of an anionic pathway in anterior midgut alkalinization, and indicate that Cl^- is the principal strong anion contributing to the net acid efflux in anterior midgut. Reversible inhibition of acid and Cl^- efflux with amides provides direct evidence that CA is an important component of the alkalinization process. Similarly, reversible inhibition of acid and Cl^- efflux with DIDS are consistent with a Cl^-/HCO_3^- exchanger, although Na^+-coupled HCO_3^- transporters, Na^+-dependent Cl^-/HCO_3^- exchangers, and some of the K^+ Cl^- co-transporters would be inhibited by DIDS at this concentration. K^+- and Na^+-coupled transporters are not likely because sufficient gradients of these cations and their pharmacological suppression were not observed with K^+- and Na^+-selective SERIS-LIX electrodes (data not shown). In the presence of higher DIDS concentration, small Cl^- influxes were recorded. The data are consistent with a small transepithelial leak of Cl^- down its concentration gradient (Fig. 6, dotted line), which probably is not related to a specific Cl^- carrier because it is insensitive to DIDS. Consequently, a basal chloride channel is included in our tentative model of trans-epithelial chloride secretion (Fig. 6). Chloride channels of types I and II have been identified and characterized recently in apical membranes of Malpighian tubules of adult *A. aegypti* with the patch-clamp technique (25).

There are at least two cell types in the larval midgut epithelium—large columnar vs. smaller cuboidal cells, based on cytology (7, 26), and stable vs. decaying cells, based on electrical measurements (21). Our model (Fig. 6) is based on the average of ion concentrations within the epithelium where single cell ion concentrations were not measured, because methods are not yet completely worked out. The anion profiles obtained by CZE revealed a strong chloride concentration difference across the epithelium, chloride being low in lumen but high in blood, with bicarbonate having the inverse distribution (Fig. 2). The CZE-

measured hemolymph chloride concentrations were consistent with those found earlier by Edwards with different techniques (27), but the complete distribution profiles of chloride and bicarbonate in lumen, epithelium, and hemolymph of insects have not been reported previously.

CZE analysis showed relatively small but significant bicarbonate/carbonate differences in the tissue vs. peritrophic fluid (average 50.7 mM at pH 7.2 in the tissue versus 58.1 mM at pH 10–11 in the luminal fluid). Bicarbonate/carbonate balance is pH dependent. From the Henderson–Hasselbalch equation, the predominant species within the cells is bicarbonate (log $([H_2CO_3]/[HCO_3^-] = 4.47$ at pH_i 7.2), whereas bicarbonate/carbonate will be close to 1:1 in luminal fluid (log $([HCO_3^-]/[CO_3^{2-}] = 1$ at pH 10.33). We can use CZE data to calculate that transport of bicarbonate from cell to lumen across the apical membrane will be thermodynamically favorable at $pH_l > 9.49$. This "bicarbonate-motive force" drives HCO_3^- out of the cells in exchange for luminal Cl^-; the force increases with increasing luminal pH (pH_l) and becomes sufficient for electroneutral Cl^-/HCO_3^- exchange at $pH_l > 11.65$ (based on a Henderson–Hasselbalch calculation with measured values of Cl^- and HCO_3^-). At lower pH values the Cl^-/HCO_3^- exchanger would have to be electrophoretic. Indeed, the sodium-driven anion exchanger (NDAE1) recently cloned from *Drosophila* ". . . may not be strictly electroneutral" (23). Moreover, because alkalinization in larval mosquito midgut depends on V-ATPase activity (6) and a transepithelial voltage is present (21, 22) but no Na^+ or K^+ gradients, the proposed anion exchanger is likely to be driven by the voltage.

Apical chloride uptake appears to occur against both electrical and chemical gradients, $Cl_l^- < Cl_c^-$ (where l and c refer to the lumen and cells, respectively) and $\Delta\Psi$ is approximately -70 mV (22). By contrast, the intracellular bicarbonate concentrations are high, presumably because of its formation from metabolic CO_2 (Fig. 6). Nonenzymatic hydration of CO_2 to H_2CO_3 (dotted line) is accelerated by CA (activation energy for the reaction of OH^- with CO_2 is decreased from 50 to 26 kJ/mol, and the reaction rate is increased by a factor of $>10^6$; ref. 8). Rapid hydration of CO_2 would help to maintain the high alkalinity in anterior midgut by providing a sustained source of the weak bicarbonate anions.

Our results suggest that the principal anions in the alkalinization pathway are HCO_3^- and CO_3^{2-}, the HCO_3^- being derived from the cells by exchange for ingested Cl^-. At a measured pH near 11 almost all of the CO^{2-}-derived anions would be CO_3^{2-}. HCO_3^- dissociation could be enhanced by an apical $K^+/2H^+$ antiporter as in lumen of caterpillar gut (15) or by an anion exchanger similar to *Drosophila* NDAE1 (23). In conclusion, our physiological and analytical results clearly implicate a Cl^-/HCO_3^- anionic pathway in alkalinization of the larval mosquito midgut but its molecular mechanisms remain to be discovered.

We are grateful to Dr. Peter J. S. Smith for support of the SERIS-LIX assays at the BioCurrents Research Center in Woods Hole, MA. We acknowledge Dr. Maria del Pilar Corena and Mrs. Michelle K. Dasher for assistance with sample collections and time-lapse assays. This research was supported in part by National Institutes of Health R01 Grants AI30464 and AI22444 (to W.R.H.), AI45098 (to P.J.L.), and NS39103 and MH60261 (to L.L.M.).

1. Dadd, R. H. (1975) *J. Insect Physiol.* **21,** 1847–1853.
2. Berenbaum, M. (1980) *Am. Nat.* **115,** 138–146.
3. Martin, M. M., Martin, J. C., Kukor, J. J. & Merit, R. W. (1980) *Oecologia* **46,** 360–364.
4. Stiles, B. & Paschke, J. D. (1980) *J. Invert. Pathol.* **35,** 58–64.
5. Filippova, M., Ross, L. S. & Gill, S. S. (1998) *Insect Mol. Biol.* **7,** 223–232.
6. Boudko, D. Y., Moroz, L., Linser, P. J., Trimarchi, J. R., Smith, P. J. S. & Harvey, W. R. (2001) *J. Exp. Biol.* **204,** 691–699.
7. Zhuang, Z., Linser, P. J. & Harvey, W. R. (1999) *J. Exp. Biol.* **202,** 2449–2460.
8. Harris, D. C. (1999) *Quantitative Chemical Analysis* (Freeman, New York).
9. Smith, P. J. S., Hammar, K., Porterfield, D. M., Sanger, R. H. & Trimarchi, J. R. (1999) *Microsc. Res. Tech.* **46,** 398–417.
10. Demarest, J. R. & Morgan, L. M. (1995) *Biol. Bull.* **189,** 219–220.
11. Smith, P. J. S. & Trimarchi, J. (2001) *Am. J. Physiol. Cell Physiol.* **280,** C1–C11.
12. Senior-White, R. (1926) *Bull. Ent. Res.* **16,** 187–248.
13. Waterhouse, D. F. (1949) *Aust. J. Sci. Res.* **132,** 428–437.
14. Dow, J. A. T. (1984) *Am. J. Physiol.* **246,** R633–R636.
15. Wieczorek, H., Putzenlechner, M., Zeiske, W. & Klein, U. (1991) *J. Biol. Chem.* **266,** 15340–15347.
16. Wieczorek, H., Brown, D., Grinstein, S., Ehrenfeld, J. & Harvey, W. R. (1999) *BioEssays* **21,** 637–648.
17. Lepier, A., Azuma, M., Harvey, W. R. & Wieczorek, H. (1994) *J. Exp. Biol.* **196,** 361–373.
18. Clark, T. M., Koch, A. R. & Moffet, D. F. (1998) *Comp. Biochem. Physiol.* **121,** 181–187.
19. Klein, U., Koch, A. & Moffett, D. F. (1996) *Ion Transport in Lepidoptera* (Chapman & Hall, London).
20. Moffett, D. F. & Cummings, S. A. (1994) *J. Exp. Biol.* **194,** 341–345.
21. Clark, T. M., Koch, A. & Moffett, D. F. (1999) *J. Exp. Biol.* **202,** 247–252.
22. Clark, T. M., Koch, A. & Moffet, D. F. (2000) *J. Exp. Biol.* **203,** 1093–1101.
23. Romero, M. F., Henry, D., Nelson, S., Harte, P. J., Dillon, A. K. & Sciortino, C. M. (2000) *J. Biol. Chem.* **275,** 24552–24559.
24. Dadd, R. H. (1976) *Ann. Ent. Soc. Am.* **69,** 248–254.
25. O'Connor, K. R. & Beyenbach, K. W. (2001) *J. Exp. Biol.* **204,** 367–378.
26. Clements, A. N. (1992) *The Biology of Mosquitoes* (Chapman & Hall, London).
27. Edwards, H. A. (1982) *J. Exp. Biol.* **101,** 143–151.